

RESEARCH ARTICLE

Open Access



Establishing a common instantaneous center of rotation for the metatarso-phalangeal and metatarso-sesamoid joints: a theoretical geometric model based on specific morphometrics

Michael Durrant^{1*} , Lara Durrant² and Tucker McElroy³

Abstract

Background: Previous research has identified separate sagittal plane instantaneous centers of rotation for the metatarso-phalangeal and metatarso-sesamoid joints, but surprisingly, it does not appear that any have integrated the distinctive morphological characteristics of all three joints and their respective axes into a model that collectively unifies their functional motions. Since all joint motion is defined by its centers of rotation, establishing this in a complicated multi-dimensional structure such as the metatarso-phalangeal-sesamoid joint complex is fundamental to understanding its functionality and subsequent structural failures such as hallux abducto valgus and hallux rigidus.

Methods: Based on a hypothesis that it is possible to develop an instantaneous center of rotation common to all four osseous structures, specific morphometrics were selected from a sequential series of 0.5-mm sagittal plane C-T sections in one representative cadaver specimen randomly selected from a cohort of nine, seven which were obtained from the Body Donation Program, Department of Anatomy, University of California, San Diego School of Medicine, and two which were in the possession of one author (MD). All mature skeletal specimens appeared grossly normal, shared similar morphological features, and displayed no evidence of prior trauma, deformity, or surgery. Specific C-T sections isolated the sagittal plane characteristics of the inter-sesamoidal ridge and each sesamoid groove, and criteria for establishing theoretical sesamoid contact points were established. From these data, a geometric model was developed which, to be accurate, had to closely mimic all physical and spatial characteristics specific to each bone, account for individual variations and pathological states, and be consistent with previously established metatarso-phalangeal joint functional motion.

(Continued on next page)

* Correspondence: Durrantmichael@gmail.com

¹Borrego Community Health Foundation, Borrego Springs, CA 92004, USA

Full list of author information is available at the end of the article



© The Author(s). 2019 **Open Access** This article is distributed under the terms of the Creative Commons Attribution 4.0 International License (<http://creativecommons.org/licenses/by/4.0/>), which permits unrestricted use, distribution, and reproduction in any medium, provided you give appropriate credit to the original author(s) and the source, provide a link to the Creative Commons license, and indicate if changes were made. The Creative Commons Public Domain Dedication waiver (<http://creativecommons.org/publicdomain/zero/1.0/>) applies to the data made available in this article, unless otherwise stated.

(Continued from previous page)

Results: Sequential sagittal plane C-T sections dissected the metatarsal head from medial to lateral and, at approximately midway through the metatarsal head, the circular nature of the inter-sesamoidal ridge (crista) was isolated; other C-T sections defined, respectively, the elliptical characteristics of the tibial (medial) and fibular (lateral) sesamoid grooves in each specimen. A general plane model representing the most basic form of the joint was developed, and its center of rotation was established with a series of tangential and normal lines. Simplified tibial sesamoid and fibular plane models were developed next which, when combined, permitted the development of a spherical model with three separate contact points. Based on the morphometrics of each sesamoid groove and a more distally positioned tibial sesamoid, the model was modified to accurately define the center of rotation and one distinctive sagittal plane geometric and functional characteristic of each groove.

Conclusion: Consistent with our hypothesis, this theoretical geometric model illustrates how it is possible to define an instantaneous center of rotation common to all three joints while simultaneously accounting for morphometric and spatial variability. This should provide additional insight into metatarso-phalangeal-sesamoid joint complex functionality and the physical characteristics that contribute to its failure.

Keywords: Fibular sesamoid, Foot kinematics, Functional morphology, Geometric model, Instantaneous center of rotation, Metatarsal motion, Sesamoid, Sesamoid groove, Tibial sesamoid

Introduction

Due to the complexity of the metatarso-phalangeal-sesamoid joint complex (MPSJC), there are few studies that have attempted to establish its instantaneous centers of rotation (ICR); we are only aware of the following five [1–5]. Defining and integrating specific morphometrics unique to each bone and their articular surfaces is essential to determining its ICR. Any geometric model developed must have the capability of defining MPSJC motion in three planes while simultaneously permitting analysis of different sesamoid spatial arrangements and allowing for variant morphometric anomalies that may adversely affect its stability. To avoid more complex vector analysis, the model presented here is simplified by aligning the metatarsal, proximal phalanx, and both sesamoids in the sagittal plane, with the understanding that it must also be capable of simultaneously integrating other planes of motion seamlessly. A different geometric perspective of the MPSJC has been previously presented by Yoshioka and colleagues [6]; five metatarsophalangeal joint cadaver specimens were embedded in resin which were sequentially sectioned in the sagittal plane. They established the congruent symmetrical relationships between each groove and its respective sesamoid and noted both grooves were oriented to the long axis of the metatarsal.

Methods

A sagittal cross section of the metatarsal head through its inter-sesamoidal ridge, also known as the crista (C-T section 23), in Fig. 1a, reveals a circular metatarsal head, which has been described as a convex spherical surface [4, 6–10].

A circle in the sagittal plane with two points on its perimeter is first considered; tangent lines to these points can be constructed, and their normal lines are

similarly defined as inward pointing lines perpendicular to the respective tangent. These normal lines, due to the geometry of the circle, will always intersect at the circle's center. Illustrated in Fig. 2b, this approach to determining a CR is also valid for more elliptical surfaces. By definition, elliptical is any curved surface which is less than that of a sphere of comparable size (i.e., the elliptical surface is more flat than a sphere in certain portions, similar to the ellipsoid of analytic geometry).

Next, consider a sagittal cross section, known as the tibial plane, with two contact points, A designating the contact point between the metatarsal and proximal phalanx, and B, representing the contact point between the metatarsal and tibial sesamoid. This idealized tibial plane is determined by A, B, and the requirement that the cross section resembles a spherical metatarsal head. In this simplified model, it is possible to establish a CR by locating the intersection of the normal lines of A and B, as illustrated in Fig. 3a. This CR, designated OT, defines distal metatarsal motion.

It is also possible to model the fibular plane, which is determined by contact points A and C (with the understanding that its cross section also be circular), where C is the contact point between the metatarsal and the fibular sesamoid. It is similarly possible to establish a CR, which is designated by OF (see Fig. 3b). Consistent with previous observations [4, 11–16] that position the fibular sesamoid more proximal, in comparing Fig. 3a and b, notice that the fibular sesamoid contact point at C is positioned more proximal relative to tibial sesamoid contact point B.

It is fairly easy to determine the coordinates of OT and OF with respect to the points A and B and the points A and C. These models give two separate CR—one for the

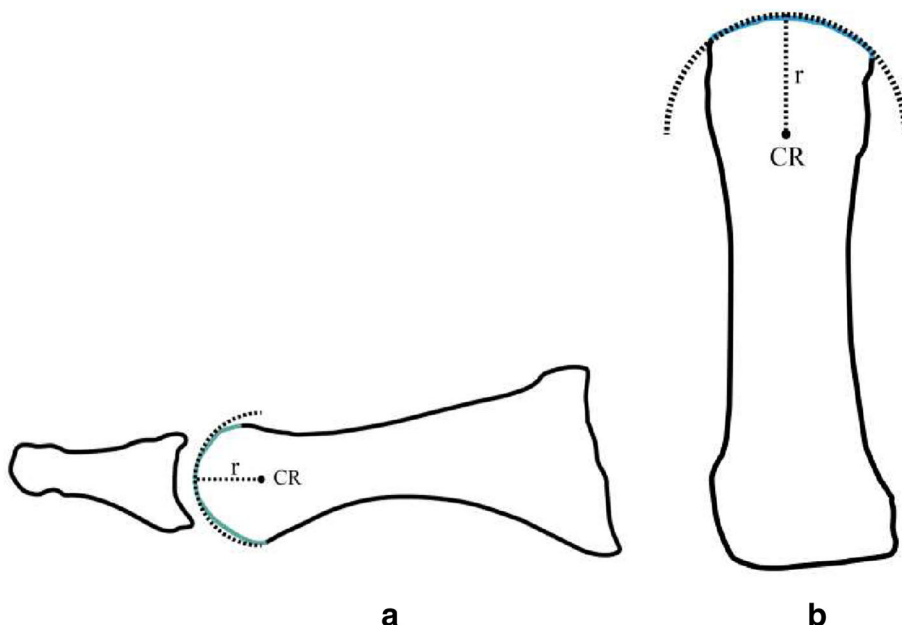
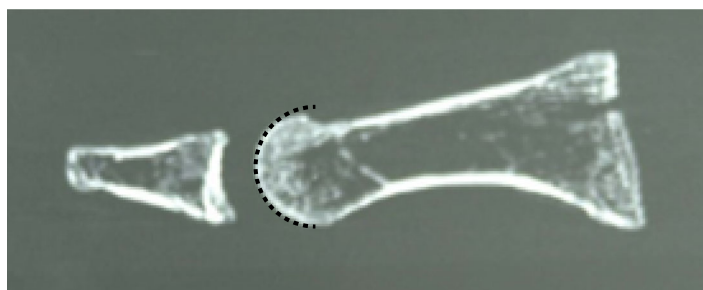


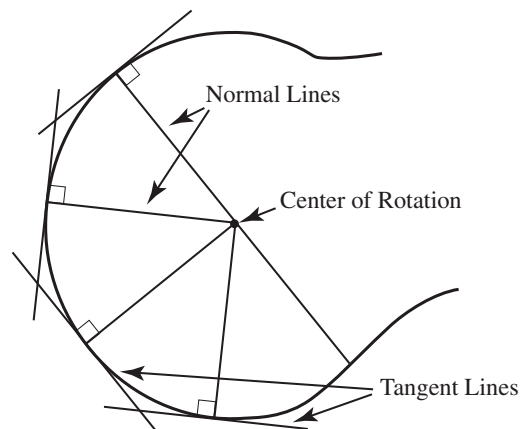
Fig. 1 A sagittal plane shadow drawing of C-T section 23, midway through the metatarsal specimen, defining its inter-sesamoidal ridge (crista), is illustrated in Figure **a**. Its distal cartilaginous surface, highlighted in teal, has been described as a convex spherical surface ([7, 4, 8, 9, 6, 10]). Figure **b** is a shadow drawing of the same metatarsal specimen from a dorsal perspective, highlighting its circular form in the transverse plane. A black dotted semi-circle (first described by Stokes and colleagues [11]), with its center of rotation designated CR, has been superimposed over the distal metatarsal edge in the sagittal and transverse planes to illustrate its distal spherical surface. The length of radius in figure 1b is slightly longer than 1a, which results in its distal surface being more flattened in the transverse plane than the sagittal plane figure in 1a. Although both images exhibit two geometrically different convex circular surfaces, it is possible to integrate both CR into one functional model

tibial plane, representing rotation about an axis perpendicular to the tibial plane, and one for the fibular plane, which represents rotation about an axis perpendicular to the fibular plane. While each of these models is less complicated than a three-dimensional model, they can account for two CR.

It is necessary for this model to account for multiple metatarsal declination angles that define its sagittal plane position at any instant of time. These angles are referenced to a stationary proximal phalangeal base, designated as A. This angle is determined by finding the angle subtended between the normal



a



b

Fig. 2 C-T section 23 in **a** is the approximate midpoint through the metatarsal head, at the inter-sesamoidal ridge in our specimen. **b** illustrates a general circular plane model denoting the distal C-T section 23 in **a**. Note that normal lines drawn perpendicular to tangential lines define its borders and help establish a CR. These normal lines, due to the geometry of the circle, will always intersect at the circle's center

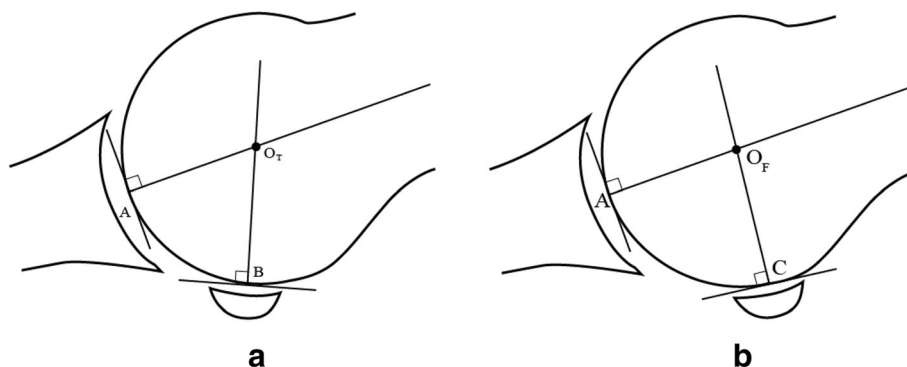


Fig. 3 **a** illustrates a tibial plane model, with normal lines drawn perpendicular to tangential lines intersecting contact points for the tibial sesamoid and proximal phalanx. Their point of intersection determines its CR. **b** illustrates the fibular plane model, with specific contact points for the proximal phalanx and fibular sesamoid. Again, the intersecting normal lines define its CR. Since the fibular sesamoid contact point is more proximal, point C is also positioned more proximal (relative to the distal metatarsal edge) than point B in **a**

line from A and the longitudinal axis of the metatarsal. This angular relationship between the two bones helps determine the initial direction and variable amount of compressive force projected toward the metatarsal from distal during stance and propulsive gait. Multiple authors have established an initial metatarsal declination angle range of 12–20° [17–22]. This initial declination is designated θ_0 and is illustrated in Fig. 4a; the CR is designated O.

The final angle, when the metatarsal has reached its highest declination angle, is designated θ_M and illustrated in Fig. 4b. This declination angle is uniquely variable with each individual and has been determined to be 65–75° [4, 17, 19, 22–26]. In between the initial angle θ_0 and θ_T , there are multiple declination angles that describe the metatarsals precise position at every second from static stance to end stage propulsion and toe off.

Results

The two axes of rotation that were established for the tibial and fibular planes in Fig. 3a and b can now be integrated, and their point of intersection is defined as their shared ICR (Fig. 5). This sphere of rotation is dictated by the geometry of the distal metatarsal surface, which may shift at any second as it rotates. Obviously, if the metatarsal head is perfectly spherical, this point will not change, but when the curvature of the metatarsal head is altered (i.e., its plantar elliptical grooves), it is possible for the instantaneous sphere of rotation to simultaneously shift in any direction. Frick [18], and somewhat later Steinler [27] both observed three planes of motion in the metatarsophalangeal joint which require three separate axes. Other researchers have also noted the capability of a shallow ball and socket joint to similarly facilitate multi-planes of motion simultaneously [4, 8, 28, 29] (Fig. 5).

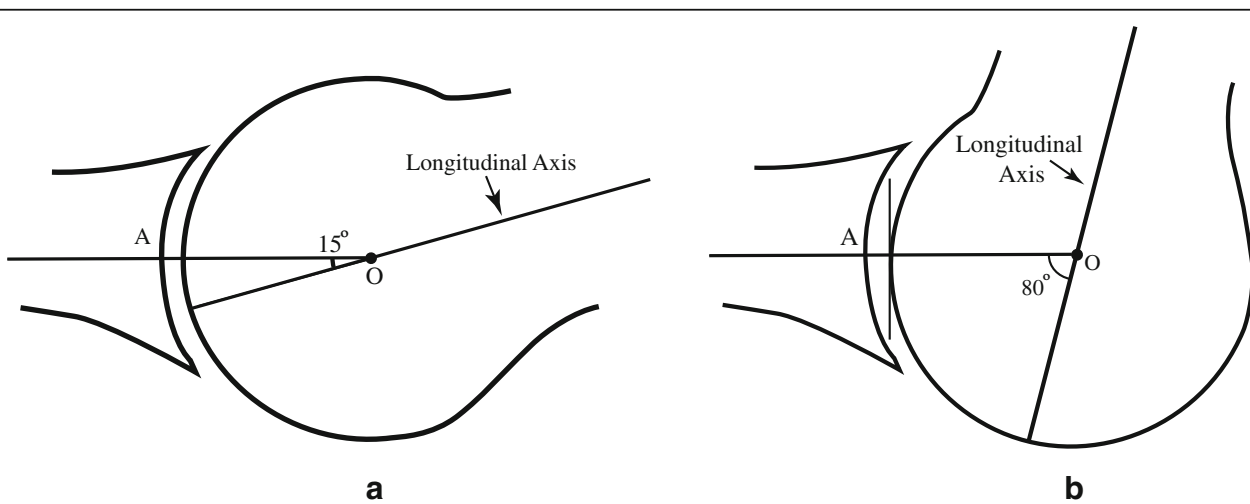
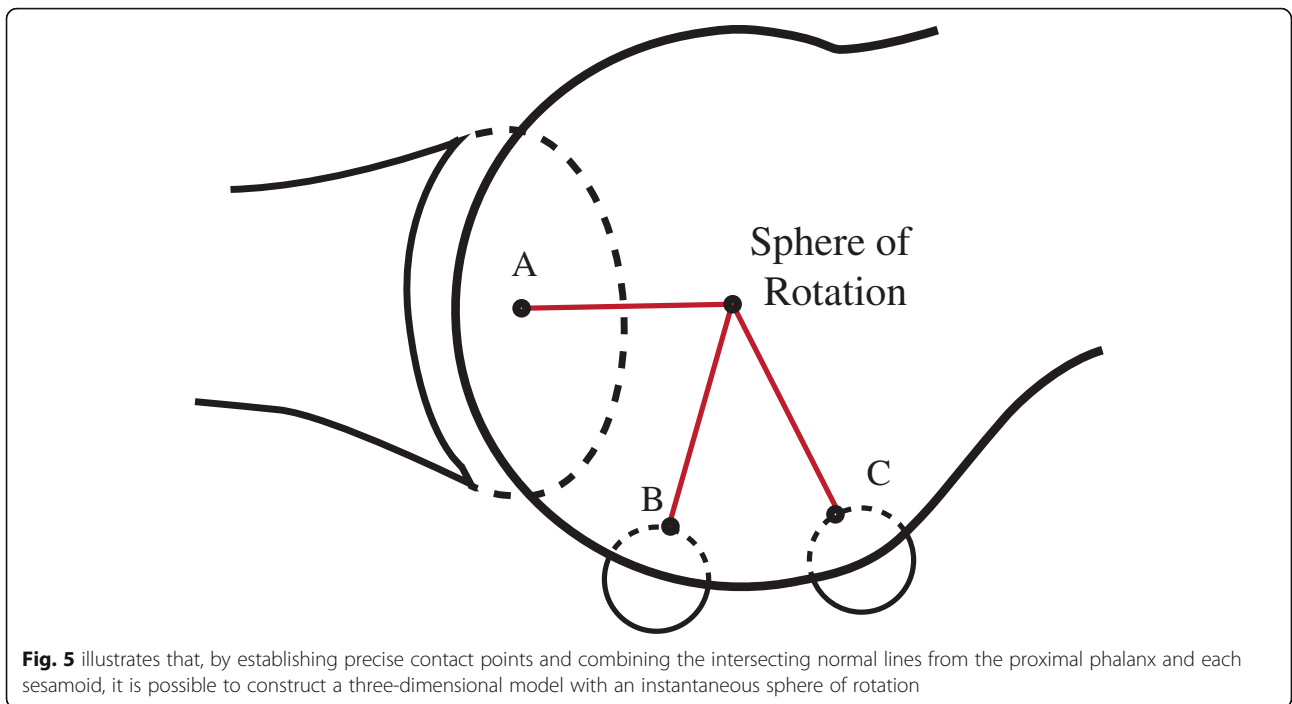
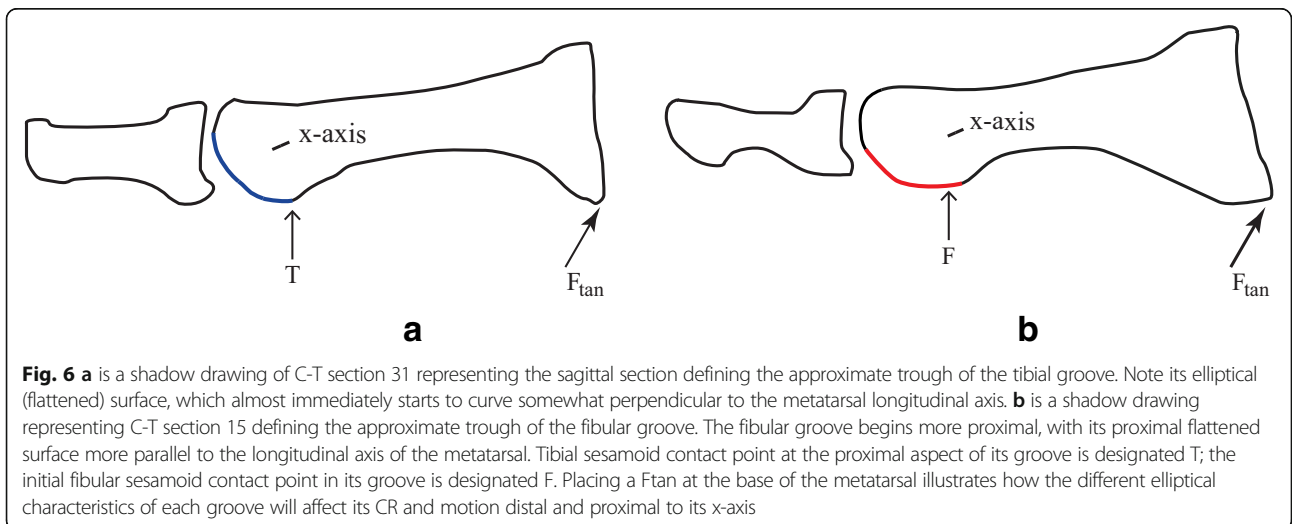


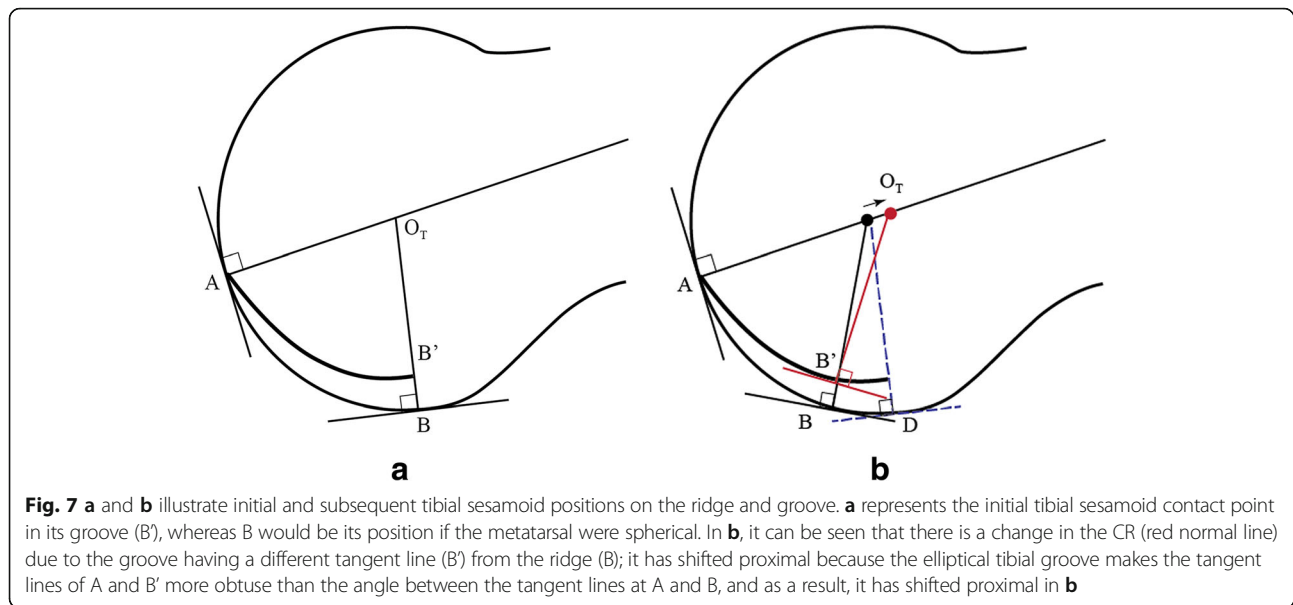
Fig. 4 **a** represents an initial 15° metatarsal declination angle, and **b** illustrates its approximate terminal declination angle



This model is consistent with observations that have described the sesamoids and proximal phalanx as a single anatomical and functional apparatus (platform) over which the metatarsal head rotates [7, 13, 30, 31] and is its base of support. Although yet to be determined in the MPSJC, research has demonstrated that it is possible to define precise contact points between adjacent bones [32–34]. This model is constructed in a manner supportive of a position that the metatarsal, with very small exceptions, is the only structure in the MPSJC that exhibits measurable motion during

propulsion [35, 36]. And because all closed chain metatarsal motion is passive [18, 27], it is possible to define its motion primarily by forces projected to its cartilaginous surface by both sesamoids and proximal phalanx. As constructed, this theoretical model will also accommodate randomly selected contact positions and, by nature of its ICR capacity, is capable of accommodating variable sesamoid sizes and spatial arrangements, different metatarsal and phalangeal lengths and declination angles, and multiple planes of motion.





Discussion

The basic principles of this geometric model can be expanded to incorporate the uniquely different elliptical characteristics of each tibial and fibular groove, which were isolated by select sagittal C-T sections of this skeletal specimen. The approximate trough of each groove was isolated and determined to be C-T section 31 for the tibial groove and CT section 15 for the fibular groove; their shadow drawings are illustrated in Fig. 6a and b.

To simplify the models in Fig. 6a and b, it is necessary to select a contact point which is constant and can be consistently defined in every individual; the proximal inception point of each sesamoid groove was used as a reference, designated T and F in Fig. 6a and b.

Defining the distal surface of the metatarsal by a series of tangent lines that follow the metatarsal head and tibial and fibular grooves rather than the inter-sesamoidal ridge, and utilizing normal lines, the intersection of points A and B (focusing on the tibial contact point) respectively will initially begin and end in the same position as does the spherical model of the metatarsal head (see Fig. 7a, which gives a depiction of the tibial contact point). Figure 7a shows that there is no difference in the CR between a model in which the sesamoid is on the ridge or in its groove, since the tangent lines are parallel at both contact points B and B'. But in Fig. 7b, these tangent lines are no longer parallel; when the sesamoid contact point is positioned further distal in its groove, its CR is actually more proximal than in the former case. This demonstrates the effect of groove curvature on the location of the CR. Figure 7a depicts the tibial contact point, but the fibular contact point is similar in principle, although it is actually positioned more proximal.

Figure 7b demonstrates how the normal line at B' is significantly altered from the normal line at B. There must exist a range of declination angles for which the tangent lines at B and B' are no longer parallel; the angle subtended between the tangent lines of A and B' is more obtuse than the angle between the tangent lines at A and B. The result of this difference between the tangent lines at B and B' is that the normal line at B' is pointed more proximal than the normal line at B. Since the normal line at B' is initially pointed in the same direction as B's normal line, there must be a shift in this normal line as the tibial groove rotates over the tibial sesamoid. Assuming that the normal line at contact point A is fixed (which depends on the implicit sphericity of the metatarsal head), the tibial CR must shift proximal. Of note, near the metatarsal's highest declination angle, the contact points B and B' will once again be identical, since groove depth will have completely diminished by then. This requires the medial CR to shift distal, close to its original position. (Fig. 8).

While the anatomical shape and curvature of the metatarsal are not as precise as in our geometric model, we have chosen to model it in this more simplistic form in order to determine its CR. Models are simplified inaccurate pictures of reality, but are useful to the extent that they capture the structure's salient features in a tractable form. The models in Fig. 7a and b gives a simplified view of the tibial plane, and illustrates how its CR will initially shift proximal, and then will shift distal later. However, since the fibular sesamoid is located (when referenced to the distal metatarsal edge) proximal to the tibial sesamoid, it follows that OT will shift proximal prior (in the course of propulsion) to the shift of OF .

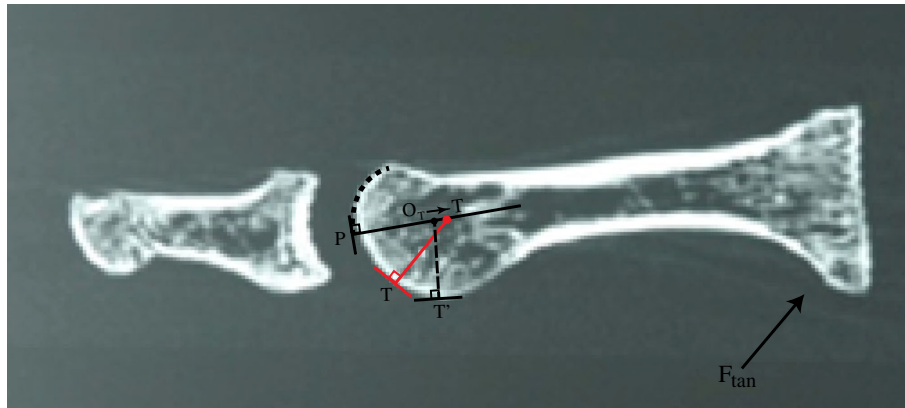


Fig. 8 is the enlarged sagittal C-T section 31 illustrating the approximate tibial groove trough in shadow drawing 31 in Fig. 6a. We have taken the concept illustrated in Fig. 7a and b and applied it to this image. An assumption is made that the tibial groove commences immediately, where its elliptical surface changes direction. The dotted black line defines the partial circular shape of the distal dorsal metatarsal edge. The CR will shift proximal in response to the geometry of the tibial groove rather than the phalanx

When Fig. 9b is examined, it can be easily seen that the flattened portion of the fibular groove begins at its proximal inception point, so that the elliptical portion of its groove appears to be more parallel to the metatarsal longitudinal axis. It is here at the distal portion of its groove that the normal line at B' is significantly altered from the normal line at B. Again, there must exist a range of metatarsal declination angles for which the tangent lines at B and B' are no longer parallel; the angle subtended between the tangent lines of A and B' is now more acute than the angle between the tangent lines at A and B (see Fig. 9b). The result of this difference between the tangent lines at B and B' is that the normal line at B' is pointed more distal than the normal line at B. Keeping in mind that the normal line at B' is initially pointed in the same direction as B's normal line, this

implies a shift in the normal line as the fibular groove rotates over its sesamoid. Assuming that the normal line at contact point A is fixed (which depends on the assumed sphericity of the metatarsal head), the fibular center of rotation must shift distal. Furthermore, near the highest metatarsal declination angle, contact points B and B' will be identical because groove depth will have diminished by this point; this will result in the fibular CR again shifting proximal, close to its original position (Fig. 10).

Figure 7a and b give a simplified view of the tibial plane and illustrate that the tibial CR will shift proximal. However, since the fibular sesamoid is positioned more proximal (Figures 9a and 9b) than the tibial sesamoid, OT will shift prior to the shift of OF.

There are multiple benefits to a distal shift in the sesamoids CR—it better aligns with the intrinsic plantar

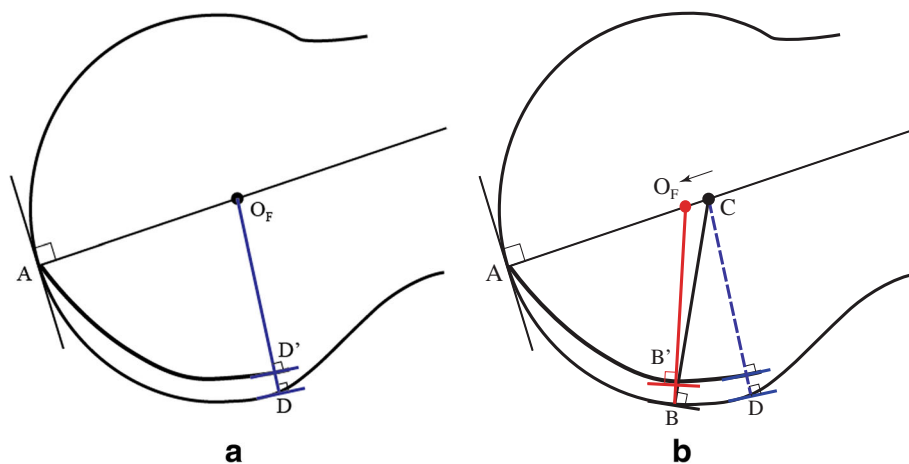


Fig. 9 a, the fibular sesamoid contact point has been placed at the proximal end of its groove. **b**, it can be seen that there is a change in the CR due to the groove having a different tangent line (B') from the ridge (B). It has shifted distal in **b**

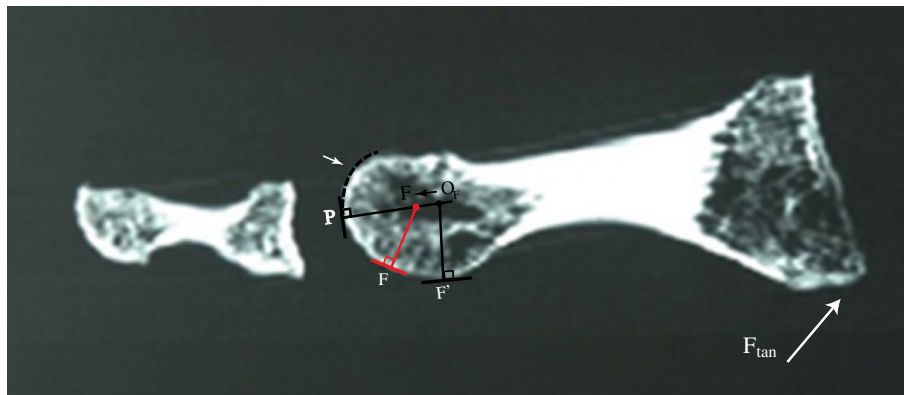


Fig. 10 is the C-T section defining the approximate trough of the fibular groove; its shadow drawing 15 is visible in Fig. 6b. We have taken the concept illustrated in Fig. 9a and b and applied it to this image; note that the CR has shifted distal. An assumption is made that the fibular groove commences immediately, where its proximal flat surface begins. Similar to the tibial shadow section, the white arrow delineates the partial circular morphometric shape of the distal dorsal aspect of the metatarsal

tendons and sesamoids at higher metatarsal declination angles. It significantly reduces the angular and rotational surface velocities of the distal metatarsal edge, while increasing them slightly at its proximal end. And importantly, it increases the amount of force required to displace the metatarsal head dorsally, thereby diminishing the prospect of a metatarsus elevatus from occurring.

There is substantial evidence that certain aberrant morphological characteristics and spatial arrangements increase the risk of hallux limitus (HL), hallux rigidus (HR), and hallux abducto valgus (HAV), and for this model to be credible, its ICR must be capable of responding to abnormalities. A flattened distal metatarsal articular surface increases the potential for linear plane deformities such as HL and HR by keeping both the phalanx and metatarsal functionally aligned in the sagittal plane [37]. Hetherington et al. [4] observed 2° of metatarsal abduction as the metatarsal, distal to its x -axis, plantarflexed; the ICR in this model would be able to accommodate this transverse plane motion. Proximally positioned sesamoids [5, 14–16, 38, 39] have been implicated in HL and HR deformities; these spatial positions will result in increased compressive shear forces between their dorsal surfaces and the metatarsal grooves at higher declination angles. Restricting end range metatarsal plantarflexion distal to its x -axis (see Fig. 6a, b) can ultimately lead to jamming and degenerative joint disease associated with HR. The relationship between elongated metatarsals and HL and HR has been known since metatarso-phalangeal joint disorders were first investigated [23, 40–46]. If the sesamoids are positioned more proximal, relative to the distal metatarsal edge, then the ICR must also be positioned more proximal.

First noted by Inge and Ferguson [47], and validated by subsequent studies, the tibial sesamoid is normally positioned more distal [15, 16, 39, 48, 49]. Siebel [50]

first noted that this spatial relationship will place the x -axis slightly oblique to the longitudinal axis of the metatarsal; this will result in its ICR being positioned slightly more lateral proximal. Importantly, the obliquity of this x -axis helps facilitate metatarsal inversion around its longitudinal axis, which has been shown to be critical for first ray stability [8, 51–53]. Any condition that initially or subsequently places the metatarsal in an everted position increases the likelihood that its functional inversion motion will be incomplete which, over time, increases the risk for ligamentous strain, hypermobility, and HAV. Factors contributing to this frontal plane deformity include surgical excision of the tibial sesamoid [54, 55], its congenital absence [56, 57], high metaphyseal eversion torsion [58], first metatarsal pronation [59–64], and a loss in the medial longitudinal arch [60]; all scenarios place the metatarsal in an excessively everted position. A failure to surgically address high metatarsal eversion angles can result in recurrent HAV [53, 65–69]. Common to these disorders is that they all collectively position the ICR more medial plantar; each can easily be assimilated into this geometric model. A short first metatarsal has been implicated in HAV [70, 71]; because of diminished ground reactive forces (GRF), there will be inadequate forces to drive metatarsal inversion, which will result in a lack of first ray stability. In this case, the ICR will exhibit very little normal frontal or transverse plane motion. A rounded distal metatarsal edge (and diminished length of radius) has been implicated in HAV [72], which females are predisposed to [73]; the ICR will be positioned more distal resulting in more potential frontal plane motion and instability. It is also possible for this model to accommodate multiple sesamoid sizes and shapes, including hypertrophied sesamoids, all of which have also been implicated in HL, HR, and HAV [14, 39].

Conclusion

Consistent with our hypothesis, this analysis demonstrates that it is possible to assimilate specific morphometric characteristics of each bone and their spatial relationships into a geometric model of the MPSJC with a common ICR. Modifications to reflect other specific morphological features, and establishing all three axes of motion in each individual bone, including defining its ICR, are all prerequisites for precisely establishing metatarsal position at each declination angle during gait. An analysis of GRF passing through each sesamoid and the phalanx prior to being projected to specific contact points on the distal and plantar aspect of the metatarsal head should further help define its motion. Finally, it seems obvious that a more complete understanding of MPSJC functionality and the underlying etiologies of HR and HAV will require a more comprehensive orthogonal coordinating system and an expanded morphometric list to more accurately define its multiple planes of motion and ICR.

Abbreviations

CR: Center of rotation; C-T: Computed tomography; GRF: Ground reactive forces; HAV: Hallux abducto valgus; HL: Hallux limitus; HR: Hallux rigidus; ICR: Instantaneous center of rotation; MPSJC: Metatarso-phalangeal-sesamoid joint complex; OF: Fibular plane center of rotation; OT: Tibial plane center of rotation; UCSD: University of California, San Diego

Acknowledgements

We thank radiologists Ron Ott MD, and Ved Prakash MD, for their assistance with the Computed tomography; David Rapaport PhD, Professor Emeritus, Department of Anatomy, UCSD School of Medicine, for his help in securing the skeletal specimens; Body Donation Program, Department of Anatomy, University of California, San Diego School of Medicine, and the individuals and their families that donated their bodies to medical research.

Funding

None of the authors received any compensation related to this manuscript.

Availability of data and materials

The sagittal plane C-T sections of the specimen that is the subject of this analysis are available upon request. It is no longer possible to specifically identify the seven skeletal specimens that were a part of a larger cohort obtained from the UCSD Department of Anatomy.

Disclosures

This manuscript, along with several others, was uploaded to Researchgate approximately 3 years ago. It was subsequently deleted about a year later, and has not previously undergone peer review.

Authors' contributions

Some concepts developed in this manuscript were initially conceived about 30 years ago, subjected to countless revisions and four computers, one which was lost. The figures deteriorated and needed to be redrawn on at least three separate occasions—these were done by LD. MD and TM jointly developed the concepts and drafted the manuscript, and each contributed to its writing. All morphologic characteristics, including those defined by the C-T sections, and subsequent shadow images and analysis were done by MD. The first geometric models presented were a joint effort by MD and TM. TM was responsible for the concept and drawing of the geometric model in Fig. 4a. The subsequent models illustrating the center of rotation changes were a joint effort by MD and TM. LD edited the paper on several occasions and made oral and written changes to provide more clarity. All authors read and approved the final manuscript.

Ethics approval and consent to participate

provided by the Anatomical Materials Review Board, Body Donation Program, University of California, San Diego School of Medicine.

Consent for publication

Not Applicable.

Competing interests

The authors declare that they have no competing interests.

Publisher's Note

Springer Nature remains neutral with regard to jurisdictional claims in published maps and institutional affiliations.

Author details

¹Borrego Community Health Foundation, Borrego Springs, CA 92004, USA. ²Loma Linda University, Loma Linda, CA 92354, USA. ³Center for Statistical Research and Methodology, U.S. Census Bureau, Washington, D.C., USA.

Received: 1 May 2018 Accepted: 21 February 2019

Published online: 16 April 2019

References

- Shereff MJ, Benjani F, Kummer FJ. Kinematics of the first metatarso-phalangeal joint. *J Bone Joint Surg.* 1986;68:7.
- Sammarco JG. Biomechanics of the foot. Basic biomechanics of the skeletal system. Philadelphia: Lea Febiger; 1980. p. 1.
- Aper RL, Saltzman C, Brown TD. The effect of hallux sesamoid resection on flexion moment arms of the first MTP joint. *Foot Ankle Int.* 1994;15:9.
- Hetherington VJ, Carnett J, Patterson BA. Motion of the first metatarso-phalangeal joint. *J Foot Surg.* 1989;28(1):13–9.
- Camasta C. Hallux limitus and hallux rigidus. Clinical examination, radiographic findings, and natural history. *Clinics Podiatr Med and Surg.* 1996;13(3):423–48.
- Yoshioka Y, Siu DW, Cooke TD, Bryant JT, Wyss U. Geometry of the first metatarsophalangeal joint. *J Orthop Res.* 1988;6(6):878–85.
- Keikian H. In hallux valgus, allied deformities of the forefoot and metatarsalgia. Structural alteration. Philadelphia: WB. Saunders; 1965. p. 7.
- Hicks JH. The mechanics of the foot. I The joints *J Anat.* 1953;87(4):345–57.
- De Asla RJ, Delund J. In: Thordarson DB, editor. *Anatomy and biomechanics of the foot and ankle, in foot and ankle.* Philadelphia: Lippincott Williams and Wilkins; 2004. p. 3–5.
- Cwikla PS, Hetherington V, Petek J. Morphological considerations of the first metatarsophalangeal joint. *J foot surg.* 1991;31(1):3–9.
- Stokes I, Hutton JC, Stott JRR. Forces acting on the metatarsal during normal walking. *J Anat.* 1979;129:12.
- Kewenter U. Sesamoid bones of human first metatarsophalangeal joint: a clinical, x-ray, and histopathological study. *Acta Orthop Scand.* 1936;2:136.
- Gillette. Des os sésamoïdes chez l'homme. *J. Anatomy Physiology.* 1872:506–38.
- Roukis TS, Jacobs P, Dawson DM, Erdmann BB, Ringstrom JB. A prospective comparison of clinical, radiographic, and intraoperative features of hallux rigidus: short-term follow-up and analysis. *J Foot Ankle Surg.* 2002;41(3):158–65.
- Prieskorn D, Graves S, Smith RA. Morphometric analysis of the plantar plate apparatus of the first metatarso-phalangeal joint. *Foot Ankle Int.* 1993;14(4):4.
- Bogdan R, Durrant M, Bogdan S. Radiographically quantifying tibial sesamoid and fibular sesamoid distances to the distal metatarsal edge in normal and hallux limitus populations, unpublished; 2002.
- Joseph J. Range of movement of the great toe in men. *J Bone Joint Surg (B).* 1954;36(3):450–7.
- Frick I, Handbuch D. In: Jena GF, editor. *Anatomie und Mechanik d. Gelenke;* 1911.
- Nawoczenski DA, Baumhauer JF, Umberger BR. Relationship between clinical measurements and motion of the first metatarsophalangeal joint during gait. *J Bone Joint Surg Am.* 1999;81(3):370–6.
- Gentili A, Masih S, Yao L. Pictorial review: foot axes and angles. *Br J Radiol.* 1996;69(826):968–74.
- Gerbert J, Sokoloff T. *Textbook of bunion surgery.* Philadelphia: WB. Saunders; 2001.
- Buell T, Green DR, Risser J. Measurement of the first metatarsophalangeal joint range of motion. *J Am Podiatr Med Assoc.* 1988;78(9):439–48.

23. Root ML, Orien W, Weed JH. Motion of the joints of the foot: the first ray, in clinical biomechanics: volume II: Normal and abnormal function of the foot clinical biomechanics, MLRoot Ed. Vol. II 1977. Los Angeles: Clinical Biomechanics.
24. Eberhart HD, Inman V, Bresler B, McCowan TD. The principals of human locomotion, Human limbs and their substitutes. PE Klobsteg and PD Wilson, Ed. New York: Hafner Publishing Company; 1968 p.34.
25. Hopson MM, McPoil TG, Cornwall MW. Motion of the first metatarsophalangeal joint. Reliability and validity of four measurement techniques. *J Am Podiatr Med Assoc.* 1995;85(4):198–204.
26. Taranto MJ, Taranto J, Bryant A, Singer KP. Radiographic investigation of angular and linear measurements including first metatarsophalangeal joint dorsiflexion and rearfoot to forefoot axis angle. *J Foot Ankle Surg.* 2005; 44(3):190–9.
27. Steinler A. Lecture XXII: the mechanics of the foot and ankle. Springfield: Charles C Thomas; 1955.
28. Sarrafian S. Anatomy of the foot and ankle: descriptive, topographic, functional. 2nd ed. Philadelphia: Lippincott; 1993.
29. Steinler A. Kinesiology of the human body. Illinois: Charles Thomas; 1955. p. 375–6.
30. Sarrafian S. Anatomy of the foot and ankle. 3rd ed. China: Lippincott, Williams, Wilkins; 2011.
31. David RD, Delagoutte JP, Renard MM. Anatomical study of the sesamoid bones of the first metatarsal. *J Amer Podiatr Med Assoc.* 1989;79(11):9.
32. Ahn TK, Kitaoka HB, Luo ZP, An KN. Kinematics and contact characteristics of the first metatarsophalangeal joint. *Foot Ankle Int.* 1987;18:5.
33. Akalan NE, Ozkan M, Temelli Y. Three-dimensional knee model: constrained by isometric ligament bundles and experimentally obtained tibio-femoral contacts. *J Biomech.* 2008;41(4):890–6.
34. Freeman MA, Pinskerova V. The movement of the normal tibio-femoral joint. *J Biomech.* 2005;38(2):197–208.
35. Kravitz SR, LaPorta G, Lawton JH. Progressive staging classification of hallux limitus and hallux rigidus. *Lower Extremity.* 1994;1(1):55–66.
36. Laporta G, Melillo T, Olinsky D. X-ray evaluation of hallux abducto valgus deformity. *J Amer Podiatr Assoc.* 1974;64(8):544.
37. Brahm S. Shape of the first metatarsal head in hallux rigidus and hallux valgus. *J Amer Podiatr Med Assoc.* 1988;78(6):300–4.
38. Miller LF, Arendt J. Deformity of first metatarsal head due to faulty foot mechanics. *J Bone Joint Surg.* 1940;22(2):349–53.
39. Munuera PV, Dominguez G, Lafuente G. Length of the sesamoids and their distance from the metatarsophalangeal joint space in feet with incipient hallux limitus. *J Amer Podiatr Med Assoc.* 2008;98:5.
40. Mancuso JE, Abramow SP, Landsman MJ, Waldman M, Carioscia M. The zero-plus first metatarsal and its relationship to bunion deformity. *J Foot Ankle Surg.* 2003;42(6):319–326.
41. Nilsson H. Hallux rigidus and its treatment. *Acta Ortho Scand.* 1930;1:8.
42. Bryant A, Tinley P, Singer K. A comparison of radiographic measurements in normal, hallux valgus, and hallux limitus feet. *J Foot Ankle Surg.* 2000;39(1): 39–43
43. Smith SE, Roukis TS. Bone and wound healing augmentation with platelet-rich plasma. *Clin Podiatr Med Surg.* 2009;26(4):559–88.
44. Calvo A, Viladot R, Gine J, Alvarez F. The importance of the length of the first metatarsal and the proximal phalanx of hallux in the etiopathogeny of the hallux rigidus. *Foot Ankle Surg.* 2009;15:1.
45. Grady JF, Axe TM, Zager EJ, Sheldon LA. A retrospective analysis of 772 patients with hallux limitus. *J Amer Podiatr Med Assoc.* 2002;92(2):102–8.
46. Munuera PV, Dominguez G, Lafuente G, Castillo JM. Radiographic study of the size of the first metatarsal-digital segment in feet with incipient hallux limitus. *J Amer Podiatr Med Assoc.* 2007. 97 (6):460–468.
47. Viegas G. Reconstruction of hallux limitus deformity using a first metatarsal sagittal-Z osteotomy. *J foot ankle surg.* 1998;37(3):204–11.
48. Inge GA, Ferguson AB. Surgery of the sesamoid bones of the great toe: an anatomic and clinical study, with a report of forty-one cases. *Archives Surg.* 1933;27(3):466–89.
49. DuVries HL. Surgery of the foot. *Acad Med.* 1959;34(10):1055.
50. Beeson P, Phillips C, Corr S, Ribbons WJ. Cross-sectional study to evaluate radiological parameters in hallux rigidus. *Foot.* 2009;19(1):15.
51. Seibel M. Foot function: a programmed text. 1988: Williams and Wilkins.
52. Ebisui J. The first ray axis and the first metatarsophalangeal joint: an anatomical and pathomechanical study. *J Amer Podiatr Assoc.* 1968;58(4):160.
53. Kelso SF, Richie DH Jr, Cohen IR, Weed JH, Root M. Direction and range of motion of the first ray. *J Am Pod Assoc.* 1982;72(12):600–5.
54. Dayton P, Feilmeier M, Kauwe J, Hirschi J. Relationship of frontal plane rotation of first metatarsal to proximal articular set angle and hallux alignment in patients undergoing tarsometatarsal arthrodesis for hallux abducto valgus: a case series and critical review of the literature. *J Foot Ankle Surg.* 2013;52(3):348–54.
55. Mann RA, Wapner KL. Tibial sesamoid shaving for treatment of intractable plantar keratosis. *Foot ankle.* 1993;13:3.
56. Coughlin M. Sesamoid pain: causes and surgical treatment. In: Instruction course lectures, vol. 39: American Academy of Orthopedic Surgeons; 1990. p. 3.
57. Day F, Jones PC, Gilbert CL. Congenital absence of the tibial sesamoid. *J Amer Podiatr Med Assoc.* 2002;92(3):153–4.
58. Zinsmeister B, Edelman R. Congenital absence of the tibial sesamoid: a report of two cases. *J foot surg.* 1985;24(4):266.
59. Durrant MN, McElroy T, Durrant L. First metatarsophalangeal joint motion in Homo sapiens: theoretical association of two-axis kinematics and specific morphometrics. *J Am Podiatr Med Assoc.* 2012;102(5):374–89.
60. Eustace S, Byne JO, Beausang O, Codd M, Stack J, Stephens MM. Hallux valgus, first metatarsal pronation and collapse of the medial longitudinal arch: a radiographic correlation. *Skelet Radiol.* 1994;23:191.
61. Collan L, Kankare JA, Mattila K. The biomechanics of the first metatarsal bone in hallux valgus: a preliminary study utilizing a weight bearing extremity CT. *Foot Ankle Surg.* 2013;19(3):155–61.
62. Shereff MJ. Pathophysiology, anatomy, and biomechanics of hallux valgus. *Orthopedics.* 1990;13(9):939–45.
63. Saltzman CL, Brandser EA, Anderson CM, Berbaum KS, Brown TD. Coronal plane rotation of the first metatarsal. *Foot Ankle Int.* 1996;17(3):157–61.
64. Inman V. Hallux valgus: a review of etiological factors. *Orthop Clin North Am.* 1974;5:8.
65. Kay DB, Njus G, Parrish W, Theken P. Basilar crescentic osteotomy. A three-dimensional computer simulation. *Orthopedic clinics N America.* 1989;20(4):571–82.
66. Talbot KD, Saltzman CL. Hallucal rotation: a method of measurement and relationship to bunion deformity. *Foot Ankle Int.* 1997;18(9):550–6.
67. Kim Y, Kim JS, Young KW, Naraghi R, Cho HK, Lee SY. A new measure of tibial sesamoid position in hallux valgus in relation to the coronal rotation of the first metatarsal in CT scans. *Foot Ankle Int.* 2015;36(8):944–52.
68. Mortier JP, Bernard JL, Maestro M. Axial rotation of the first metatarsal head in a normal population and hallux valgus patients. *Ortho & Trauma: Surg & Research.* 2012;98(6):677–83.
69. Okuda R, Yasuda T, Jotoku T, Shima H. Proximal abduction-supination osteotomy of the first metatarsal for adolescent hallux valgus: a preliminary report. *J OrthoScience.* 2013;18(3):419–25.
70. Morton D. The human foot. New York: Columbia University Press; 1935.
71. Harris RI, Beath T. The short metatarsal its incidence and clinical significance. *J Bone Joint Surg [B].* 1949;31(3):13.
72. Heden RI, Sorto LA Jr. The buckle point and the metatarsal protrusion's relationship to hallux valgus. *J Amer Podiatr Med Assoc.* 1981;71(4):200–8.
73. Ferrari J, Hopkinson DA, Linney AD. Size and shape differences between male and female foot bones: is the female foot predisposed to hallux abducto valgus deformity? *J Amer Podiatr Med Assoc.* 2004;94(5):434–52.

Ready to submit your research? Choose BMC and benefit from:

- fast, convenient online submission
- thorough peer review by experienced researchers in your field
- rapid publication on acceptance
- support for research data, including large and complex data types
- gold Open Access which fosters wider collaboration and increased citations
- maximum visibility for your research: over 100M website views per year

At BMC, research is always in progress.

Learn more [biomedcentral.com/submissions](https://www.biomedcentral.com/submissions)

